NANO · MICRO small
www.small-journal.com

Degradation Kinetics of Organic–Inorganic Hybrid Materials from Micro-Raman Spectroscopy and Density-Functional Theory: The Case of β-ZnTe(en)$_{0.5}$

Tang Ye, Yi-Yang Sun, Margaret Kocherga, Andrei Nesmelov, Thomas A. Schmedake, and Yong Zhang**

Organic–inorganic hybrid materials often face a stability challenge. β-ZnTe(en)$_{0.5}$, which uniquely has over 15-year real-time degradation data, is taken as a prototype structure to demonstrate an accelerated thermal aging method for assessing the intrinsic and ambient-condition long-term stability of hybrid materials. Micro-Raman spectroscopy is used to investigate the thermal degradation of β-ZnTe(en)$_{0.5}$ in a protected condition and in air by monitoring the temperature dependences of the intrinsic and degradation-product Raman modes. First, to understand the intrinsic degradation mechanism, the transition state of the degradation is identified, then using a density functional theory, the intrinsic energy barrier between the transition state and ground state is calculated to be 1.70 eV, in excellent agreement with the measured thermal degradation barrier of 1.62 eV in N_2 environment. Second, for the ambient-condition degradation, a reduced thermal activation barrier of 0.92 eV is obtained due to oxidation, corresponding to a projected ambient half-life of 40 years at room temperature, in general agreement with the experimental observation of no apparent degradation over 15 years. Furthermore, the study reveals a mechanism, conformation distortion enhanced stability, which plays a pivotal role in forming the high kinetic barrier, contributing greatly to the impressive long-term stability of β-ZnTe(en)$_{0.5}$.

1. Introduction

Organic–inorganic hybrids may offer material properties enhanced compared to or not available from their inorganic and organic component.[1–3] However, they are typically less stable than the inorganic counterparts. Because practical operation of a device requires it to be resistive to the common paths of degradation (e.g., oxidation), understanding the hybrids' stability in both protected and ambient conditions becomes critical.

Interest in hybrid materials has skyrocketed in the last decade or so, because the rapid development of organic–inorganic hybrid perovskite $MAPbI_3$ (MA = $CH_3NH_3^+$) and its derivatives have shown unprecedented potential for a wide range of applications, including photovoltaics and solid-state lighting. Unfortunately, despite the impressive improvement in stability in recent years, currently reaching a few months, achieved by surface passivation and reduction of structural defects,[4–7] they remain inadequate for general (opto)electronic applications that expect a usable life of 10–20 years. It remains uncertain whether the stability of the hybrid perovskites can be drastically improved further (e.g., beyond 10 years). Therefore, it is highly desirable to have an accelerated thermal aging test that can offer a reasonably reliable prediction of the optimal stability limit, instead of having to wait over a decade to know the answer.

$MAPbI_3$ has been predicted to have a formation energy −0.06 eV f.u.$^{-1}$ (formula unit) for the room temperature tetragonal phase, i.e., thermodynamically unstable.[8] Nevertheless, the

T. Ye, M. Kocherga, T. A. Schmedake, Y. Zhang
Nanoscale Science
University of North Carolina at Charlotte
Charlotte, NC 28223, USA
E-mail: yong.zhang@uncc.edu

Y.-Y. Sun
State Key Laboratory of High-Performance Ceramics and Superfine Microstructure
Shanghai Institute of Ceramics
Chinese Academy of Sciences
Shanghai 201899, China
E-mail: yysun@mail.sic.ac.cn

A. Nesmelov, T. A. Schmedake
Department of Chemistry
University of North Carolina at Charlotte
Charlotte, NC 28223, USA

Y. Zhang
Department of Electrical and Computer Engineering
University of North Carolina at Charlotte
Charlotte, NC 28223, USA

The ORCID identification number(s) for the author(s) of this article can be found under https://doi.org/10.1002/smll.202302935

DOI: 10.1002/smll.202302935

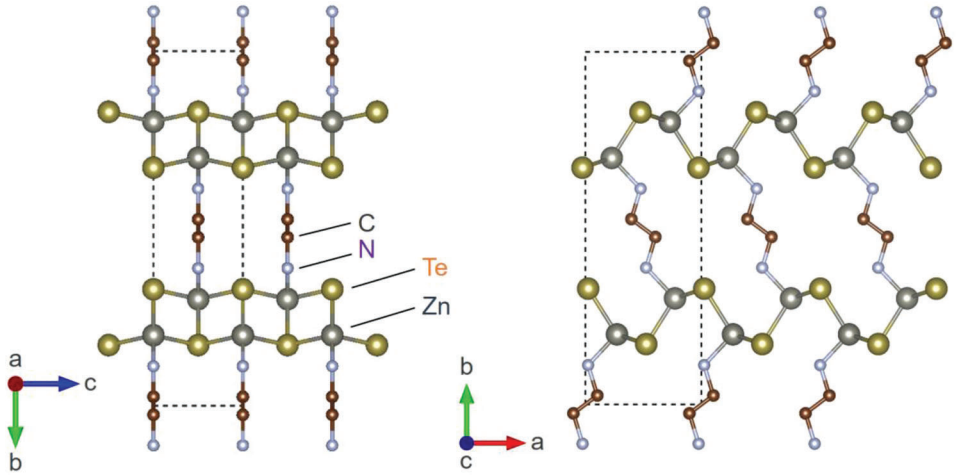

Figure 1. Crystal structure of β-ZnTe(en)$_{0.5}$ viewed along *a*- and *c*-axes.

structure is known to be stable at least for a period of time if properly protected. Thus, a modest kinetic barrier is expected, although it is not straightforward to calculate. An accelerated thermal aging experiment on bare $MAPbI_3$ films offered a half-life of 70 d in air at 60 °C with an activation energy of 0.96 eV.[9] $CsPbI_3$ is expected to be thermodynamically stable albeit the formation energy is rather small, 0.098 eV f.u.$^{-1}$, for its orthorhombic phase.[8] A recent report on accelerated thermal aging tests of $CsPbI_3$ materials and solar cells has yielded interesting results:[10] for the caped (uncapped) samples, the thermal activation energies are determined to be 0.536 (0.287) eV from the conductivity measurement and 0.487 (0.248) eV from the solar cell performance, which translates to projected 80% lifetimes about 5.8 and 0.5 years for the device at 35 °C, respectively. Since the all-inorganic version is known to be more stable than the hybrid version, one may wonder if these results set the upper limit for its hybrid counterparts. The reliability of such predictions or the methodologies is yet to be verified, as so far, the real-time aging data over even one year is not readily available for these materials.

A family of II–VI based hybrid structures[11,12] has been shown to possess various unusual or unique properties and potential applications.[13–19] As a prototype, β-ZnTe(en)$_{0.5}$ can be viewed as a superlattice with alternating layers of two-monolayer thick (110) ZnTe and single-molecule length ethylenediamine, as shown in **Figure 1**.[12,15] In contrast to all the known inorganic superlattices where interfacial diffusion is inevitable,[20,21] β-ZnTe(en)$_{0.5}$ exhibits not only an unusually high degree of crystallinity in macroscopic scale, but also shows an exceptionally low level of microscopic scale defects,[17] which has not been possible even for the very high-quality CdTe, GaAs, and hybrid perovskite $MAPbI_3$.[22] Furthermore, perhaps being the first documented example among the crystalline hybrid structures in the literature, β-ZnTe(en)$_{0.5}$ has been shown to have a unprotected shelf life over 15 years.[17]

While the focus of our recent work was investigating the manifestation of the high crystallinity and stability on the structural, electronic and optical properties, the accelerated thermal aging in a protected condition (in N_2) has yielded an activation energy > 1.6 eV for thermal degradation, and a projected intrinsic life around 10^8 years.[17] The measured high activation barrier implies the existence of a formidable but unexplained kinetic barrier, since the calculated formation energy, although much larger than the most halide perovskites,[8] was only around 0.5 eV f.u.$^{-1}$.[17] Furthermore, despite the over 15-year shelf life is impressive for a hybrid structure, the huge difference between the intrinsic lifetime and the lifetime in air is unexplained. Many III–V semiconductors are known to be air stable over many decades, such as GaP,[23] and even dislocation defects were shown remaining the same over multiple years being studied.[24] However, the stability of the II-VI hybrids has been found to be sample dependent over the time frame about 20 years in which they were monitored. The degradation could vary significantly even within one piece of sample.[17] Thus, their stability is sensitive to the extrinsic effects, such as surface and bulk defects, and the shelf life is expected to be shorter than the stable inorganic materials. While the projected 10^8-year intrinsic lifetime suggests that the long-term stability of the material is not of practical concern if the material can be properly encapsulated, it is non-trivial to experimentally verify the reliability of the prediction directly. Since β-ZnTe(en)$_{0.5}$ has already been shown to have an ambient over 15 years, a time scale important for real-world applications, it is an ideal prototype structure for validating the reliability of an accelerated thermal aging technique. Once the reliability of the methodology is established, one could then attempt to apply it to lesser stable materials where more stringent experimental controls would likely be required.

This work aims to address the two important but unsettled issues of the previous study on β-ZnTe(en)$_{0.5}$:[17] 1) whether the empirical > 15 years shelf life is actually close to the optimal ambient lifetime; 2) what the underlying mechanism is for the high kinetic barrier derived from the thermal degradation under the protected environment. These issues are pivotal to assessing the reliability of the accelerated thermal aging experiment to predict both the intrinsic and (optimal) ambient lifetime of a hybrid material or any other material whose long-term stability is of concern. The answer to the second question might provide indirect confirmation to the projected super-long lifetime that cannot be directly verified.

To address the first issue, we need to minimize the influence of the extrinsic effects, such as defects and edges. It has

been found that for the II–VI hybrids, degradation often starts at the edge of the samples.[17,25] To minimize the potential extrinsic sample inhomogeneity on the thermal degradation, we apply a localized probing technique that monitors the degradation of an interior region sufficiently away from any edge and free of obvious surface defect, which is more reliable than a technique probing the whole sample, as done in the past for the perovskites.[9,10] It is also desirable to use a technique that only causes minimal perturbation to the sample, for instance, Raman spectroscopy using excitation energy below the bandgap, since above-bandgap excitation often leads to photodegradation of the hybrid materials.[26] Specifically, we monitor the thermal degradation at various elevated temperatures in air by measuring the decay of the hybrid Raman modes as well as the build-up of the Raman signal of the degradation product, and further using two degradation models to extract the relevant parameters and predict the idealistic ambient lifetime (at room temperature).

To address the second issue, we need to identify the appropriate transition state that dictates the kinetic barrier. The previous thermal degradation study under the protected condition has indicated that the intrinsic degradation path is the separation of the organic and inorganic component, resulting in losing the molecules and the formation of bulk ZnTe. By recognizing that the transition state could be the state when the molecule and ZnTe slab are just separated but retaining the respective structures in the crystal, we are able to calculate the kinetic barrier, using the density-functional theory (DFT), in excellent agreement with the measured activation energy. Significantly, we reveal a key mechanism that increases the kinetic barrier, that is, the structural distortions relative to the free states of the molecule and inorganic slab increases the kinetic barrier. This mechanism should be an important consideration for improving the stability of any superstructure that consists of different substructures.

2. Results and Discussion

Compared with the transparent, pristine β-ZnTe(en)$_{0.5}$ crystals, some over a decade old samples appeared darker in color. A combination of Raman, XPS, and SEM/EDAX study on those darker samples confirmed the existence of a mixture of oxidation products, including tellurium and/or tellurium oxide, but the degradation features were found only on the sample surface, within 2 μm from the crystal-air boundary even for the most degraded samples.[17] Furthermore, thermogravimetric analysis (TGA) study suggested that the degradation was a convolution of multiple competing oxidation processes: β-ZnTe(en)$_{0.5}$ → $ZnTeO_2$, where $ZnTeO_2$ is predominantly a mixture of ZnO + xTe + yTeO + $z$$TeO_2$ ($x + y + z = 1$), as revealed by Raman spectra of the degradation products.[17] As will be shown, although the degradation in ambient air involves multistep oxidation, an effective reaction barrier can still be measured, and it remains relatively large, consistent with the observed long ambient lifetime. For reference, we first study the intrinsic degradation where the hybrid decomposes into bulk ZnTe and en molecules: β-ZnTe(en)$_{0.5}$ → ½ en + ZnTe. It is of great importance to study the intrinsic degradation because first, the intrinsic degradation, as we will show, can be viewed as a simple one-step reaction. The simplicity of the reaction allows one to propose a well-defined transition state and clarify different possible contributions to its kinetic barrier. Second, the insights obtained from intrinsic degradation can be transformed to the ambient degradation.

2.1. Intrinsic Degradation and Its Activation Barrier

Removal of the oxidation agents allows one to observe the intrinsic degradation. In situ Raman measurements at different target temperatures are performed in N_2 with a confocal Raman system, which allowed us to monitor and quantify the reaction process, and estimate the activation barrier of intrinsic degradation.[17] For each temperature, one piece of pristine β-ZnTe(en)$_{0.5}$ crystal is used and the spectra are taken, using confocal micro-Raman, from a location away from the sample edge with clean surface. The sample is heated from room temperature directly to a target temperature. The sample change is assumed to be negligible during the short heating process. While being kept at the target temperature, the Raman signal from a fixed volume (determined by the optical system) near the top of crystal is recorded as a function of time. If a material property is defined as $P(T,t)$, T being the temperature and t being the exposure time for the sample at T, then to a first approximation, TGA probes $P(T,t = 0)$ and the in situ Raman monitors $P(T = T_0, t)$, with T_0 being the set temperature. For β-ZnTe(en)$_{0.5}$, based on the fact that a partial or fully degraded sample shows weakened or disappeared en derived Raman modes,[17] we may understand the degradation process as losing en molecules from the structure. **Figure 2**A shows schematically how the reaction progresses at different times while Raman measurements are performed continuously. At $t = 0$, because the crystal structure is nearly at its pristine state, the hybrid Raman peaks are at their highest intensities. As en molecules leave the structure, the amount of hybrid crystal in the probed volume diminishes. Hence the hybrid Raman peaks decay. Eventually, when there is almost no hybrid structure left in the probed volume, hybrid Raman modes will become nonobservable.

As examples, shown in **Figure 3**A are the Raman spectra at 225 °C measured at selected delay times when the degradation process is relatively slow. At $t = 0$, the spectrum resembles that of a pristine sample at room temperature other than some changes in peak intensity and position, and the Raman signal of the degradation product (i.e., the ZnTe peaks) is minimal. As en molecules leave the structure over time, the ZnTe peaks become more prominent. Here, we use the Raman decay from the strongest hybrid mode at 133 cm^{-1} to monitor reaction progress. Figure 3B depicts the normalized peak intensity $A(t)$ versus time for the hybrid mode at 133 cm^{-1} and the growing ZnTe LO phonon mode at 201 cm^{-1} at 225 °C.

To extract the degradation parameters, we use the data obtained at temperatures between 210 and 270 °C. Figure 3C,D shows the $A(t)$ curves for the hybrid Raman mode for a few representative temperatures in linear and logarithmic scale (the complete data set are given in SM1, or Figure S1, Supporting Information). As shown, they can be fit well with an exponential decay, indicating the thermal degradation is a one-step

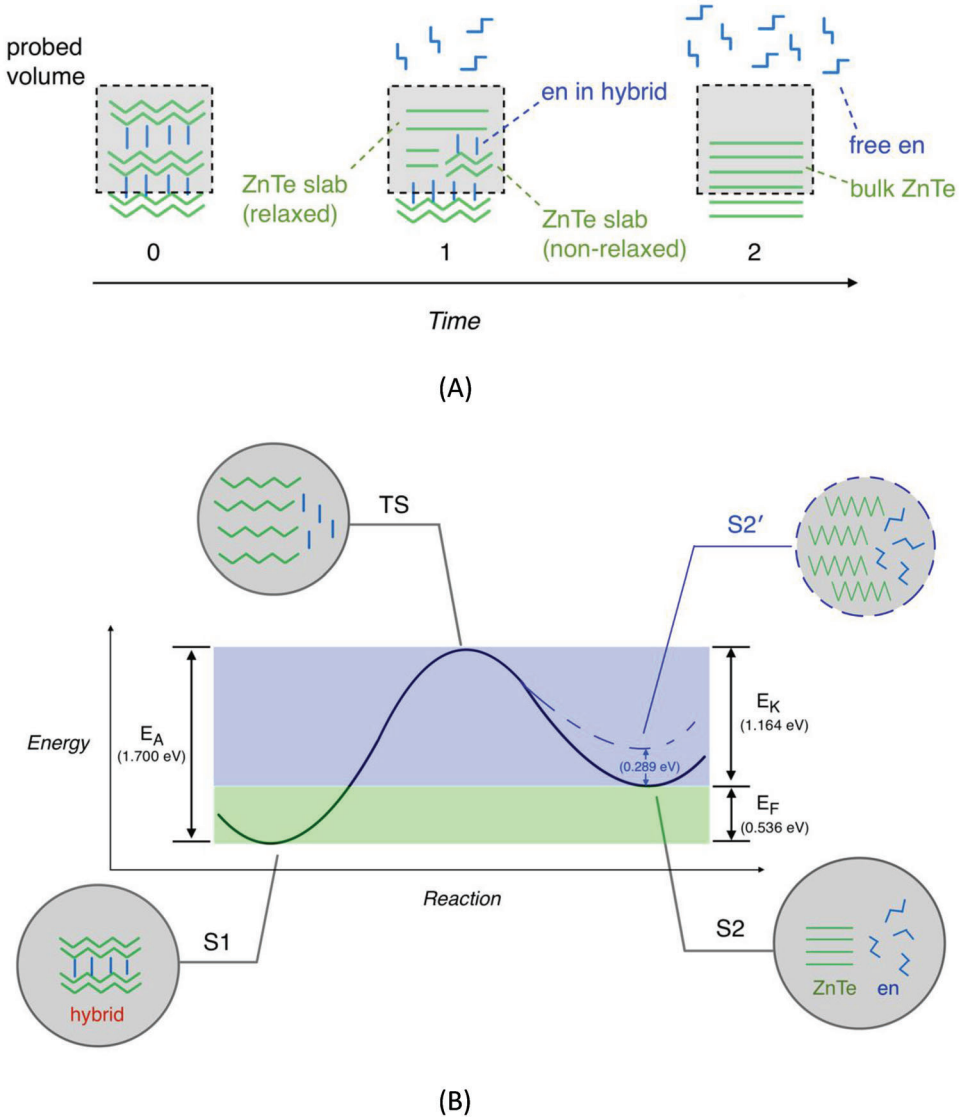

Figure 2. Degradation kinetics of β-ZnTe(en)$_{0.5}$. A) A schematic for monitoring the reaction progress. Raman signal comes from a fixed volume in which initial state ($t = 0$) is the pure hybrid crystal. As the reaction progresses ($t = 1$), only part of the volume remains as the hybrid. Eventually ($t = 2$), there is no hybrid left in the detected volume. B) The energy landscape of the thermal degradation. The vertical axis is energy. The horizontal axis depicts possible states in the reaction progress. From left to right are: S1, refers to the state of a pristine hybrid; TS, refers to the transition state that S1 must overcome to reach S2 (bulk ZnTe and free en molecules) or S2′ (freestanding ZnTe slabs and en molecules). In the energy landscape, formation energy (E_F) is highlighted in green, and the barrier in excess of the formation energy (E_K) is highlighted in blue. The labeled energy changes are derived from the DFT calculations.

decomposition and can be described using a simple first-order kinetic model

$$A(T, t) = \exp[-k(T)\,t] \quad (1)$$

$$k(T) = C \exp\left(-\frac{E_A}{k_B T}\right) \quad (2)$$

Figure 3E shows the results using the Arrhenius relationship to estimate the activation energy E_A and pre-factor C by fitting $\ln(k)$ versus $1/T$. The fitting yield $E_A = 1.62 \pm 0.08$ eV, $\ln(C) = 27.2 \pm 1.9$ (C in s^{-1}). The lifetime $t_{1/2}$, measured by the decay time of the hybrid Raman mode intensity reaching 50% of the $t = 0$ value, can be calculated at each temperature. Extrapolating to room temperature ($T = 300$ K), we have $\ln(k) = \ln(C) - E_A/(k_B T) = -35.5 \pm 1.3$, corresponding to a lifetime $t_{1/2}(T = 300\ \text{K}) = 8.2 \times 10^7$ (from 2.1×10^7 to 3.1×10^8) years.

Figure 2B depicts the energy landscape of the intrinsic degradation, following the transition state theory.[27] From left to right, S1 stands for the pristine state of the hybrid, TS stands for a transition state which we will define shortly, S2 stands for the state where the hybrid degrades into en molecules and bulk ZnTe. The energy difference between S1 and TS is the activation barrier in term of the Gibbs free energy (ΔG), which can be

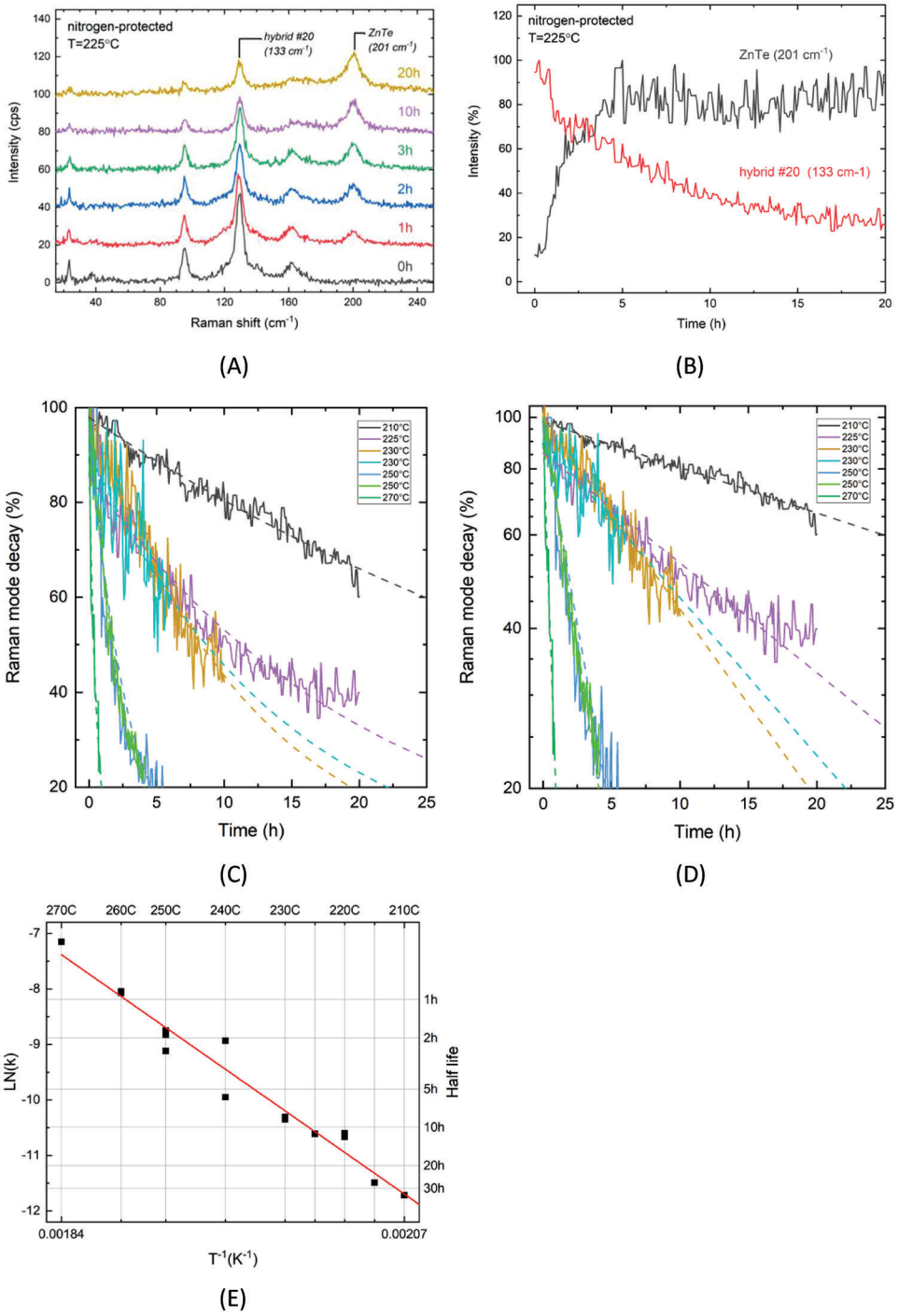

Figure 3. In situ Raman monitoring of thermal degradation of β-ZnTe(en)$_{0.5}$ in N_2 protected environment. A) Raman spectra acquired at 1, 2, 3, 10, 20 h after the hybrid sample is heated to 225 °C. B) The intensity of the hybrid mode #20 (at 133 cm^{-1}) and ZnTe (201 cm^{-1}) as a function of time. Normalized Raman peak intensity (hybrid mode #20) versus time at selected temperatures between 210 and 270 °C in N_2, in C) linear scale and D) log scale. Solid line: experimental data (in intervals of 5 min), overlapped with fitting curves (dashed line). E) Arrhenius plot of $k \propto \exp(-E_A/kT)$ versus $1/T$. Right axis labels the half-life corresponding to different values of $\ln(k)$.

further reduced into an enthalpy (ΔH) term and an entropy (ΔS) term.

$$\Delta G = \Delta H - T \times \Delta S \quad (3)$$

ΔH quantifies the net energy flow into the system during its transformation from S1 to TS. ΔS describe the entropic cost during the transformation and typically depends on the reaction cross sections. Here, in the context of a one-step decomposition process, we make two propositions. First, we propose TS be the state at the instance when the bond between the organic and inorganic component is just broken. We will show by our DFT calculations that this picture of the TS is consistent with the measured activation barrier. Second, we ignore the entropy term ΔS.[8] Under the two simplifications, the measured E_A becomes a direct measurement of ΔH or ΔU (pressure is negligible for a solid in air), the binding energy of S1 relative to TS. The transition state or degradation path is often not clearly known thus non-trivial to calculate its energy level. In this case, the transition state can be taken as the state when the en–Zn bond is just broken while the molecule and the two-monolayer thick ZnTe slab retain their respective conformations (i.e., nonrelaxed structures) in the crystal. The calculated energy difference between TS and S1 is 1.700 eV per bond or per f.u. (see SM2 in the Supporting Information for the details), which can be understood as the total thermal activation energy E_A. This value agrees very well with the experimentally obtained thermal activation energy of 1.62 eV. Taking the calculated formation energy $E_F = 0.536$ eV f.u.$^{-1}$ (see SM2 in the Supporting Information), the kinetic barrier will be $E_K = E_A - E_F = 1.164$ eV. Despite the large formation energy's contribution to the overall stability, the calculation indicates that it only accounts for about one-third of the total barrier, whereas the remaining two-third is contributed by the kinetic barrier.

It is of interest to gain more insight to the high kinetic barrier. One may envision the hybrid superlattice as stacking the inorganic slabs and en molecules. The energy state with fully relaxed molecules and ZnTe slabs, which may be viewed as intermediate degradation products, is found to be much lower than the unrelaxed state, by 0.875 eV f.u.$^{-1}$ (see SM2 in the Supporting Information for the details). The large difference indicates that significant structural distortion occurs for both components upon the formation of the hybrid crystal. This conformation distortion, resulting from the interlocking of the two components, effectively raises the kinetic barrier by a large amount of 0.875 eV f.u.$^{-1}$. Without the distortion, the kinetic barrier would be only 1.164 − 0.875 = 0.289 eV, which corresponds to the energy per formula needed to break up bulk ZnTe into the freestanding slabs. In summary, the kinetic barrier may be viewed as the sum of the three parts: breaking up the bulk ZnTe into slabs (0.289 eV f.u.$^{-1}$), the distortion of the slab (0.392 f.u.$^{-1}$), and the distortion of the molecule (0.483 eV/bond). Note that the relaxed inorganic slab and en molecule can be viewed as the substructures of the hybrid crystal, thus, their states may also be used as the reference point (S_2' in Figure 2B) for the formation energy calculation, in contrast to the common practice of using the bulk states as the references for a superlattice.[28] Using S_2' as the reference yields a formation energy of $E_F' = 0.825$ eV and kinetic barrier $E_k' = 0.875$ eV, nearly symmetric E_F and E_k.

In contrast, hybrid perovskites, such as $MAPbI_3$, particularly in their cubic phase, do not benefit from this effect, where the organic molecules have the freedom rotating in the void of the Pb–I_6 octahedra.[29] However, in the low temperature orthorhombic phase, the molecules are locked spatially and somewhat distorted, and the structure becomes slightly more stable.[8] Similarly, the layered versions of the II–VI hybrids are also less stable,[13,25] because the molecules are unconstrained on one end, thus, less distorted. This understanding reveals an important mechanism that may simultaneously enhance both the formation energy and kinetic barrier of a superstructure—the substructure distortion enhanced stability. While it is well-known that the conformation distortion of the constituents in a superstructure contributes to lowering the total energy of the system, as also discussed for the II–VI hybrids,[30,31] its role in raising the kinetic barrier has not been explicitly recognized in the literature.

2.2. Oxidation in Ambient Conditions

β-ZnTe(en)$_{0.5}$ has a large intrinsic energy barrier toward thermal degradation. However, a thermodynamically stable structure may still be environmentally unstable because molecules in ambient air may enable alternative degradation pathways with lower energy barriers. In the case of β-ZnTe(en)$_{0.5}$, we know its lifetime in ambient conditions can exceed 15 years, but we aim to obtain a reasonably reliable estimate of how much longer it can endure. For this purpose, in this section, we perform the similar measurements as done previously in N_2 now in air to investigate β-ZnTe(en)$_{0.5}$'s ambient degradation and apply what we have learned from intrinsic degradation.

Upon exposure to air, oxidation occurs on the surface of β-ZnTe(en)$_{0.5}$ but the process is self-limiting, resulting in a very thin oxide layer,[17] similar to the formation of a native oxide layer on Si. After that, the oxidation process is expected to be rather slow, providing the surface is free from additional structural defects. Nevertheless, we may expect to have a smaller E_A than intrinsic degradation because, within the similar time durations of heating, the product of oxidative degradation, tellurium, becomes observable at 160 °C, whereas the product of intrinsic degradation, ZnTe, only becomes observable when the temperature is greater than 230 °C.[17]

Figure 4 shows the results of in situ Raman experiment monitoring the reaction progress of ambient degradation and estimating its overall activation barrier. In ambient degradation, because of the accumulation of tellurium on the sample surface, in addition to the Raman decay of hybrid modes, we may also use the growing tellurium peak to monitor the reaction progress. As examples, shown in Figure 4A are the Raman spectra at 140 °C measured at selected delay times when the degradation process is slow. At $t = 0$, the spectrum resembles that of a pristine sample at room temperature other than some changes in peak intensity and position, and the Raman signal of the degradation product (i.e., the Te peaks) is minimal. As en molecules leave the structure over time, the Te peaks become more prominent. Figure 4B depicts the normalized peak intensity $A(t)$ versus time for the hybrid mode at 133 cm^{-1} and the Te mode at 121 cm^{-1}. The decay of the hybrid peak is noticeable up to the first 15 h, and becomes very slow after that, indicating that the degradation is not a single

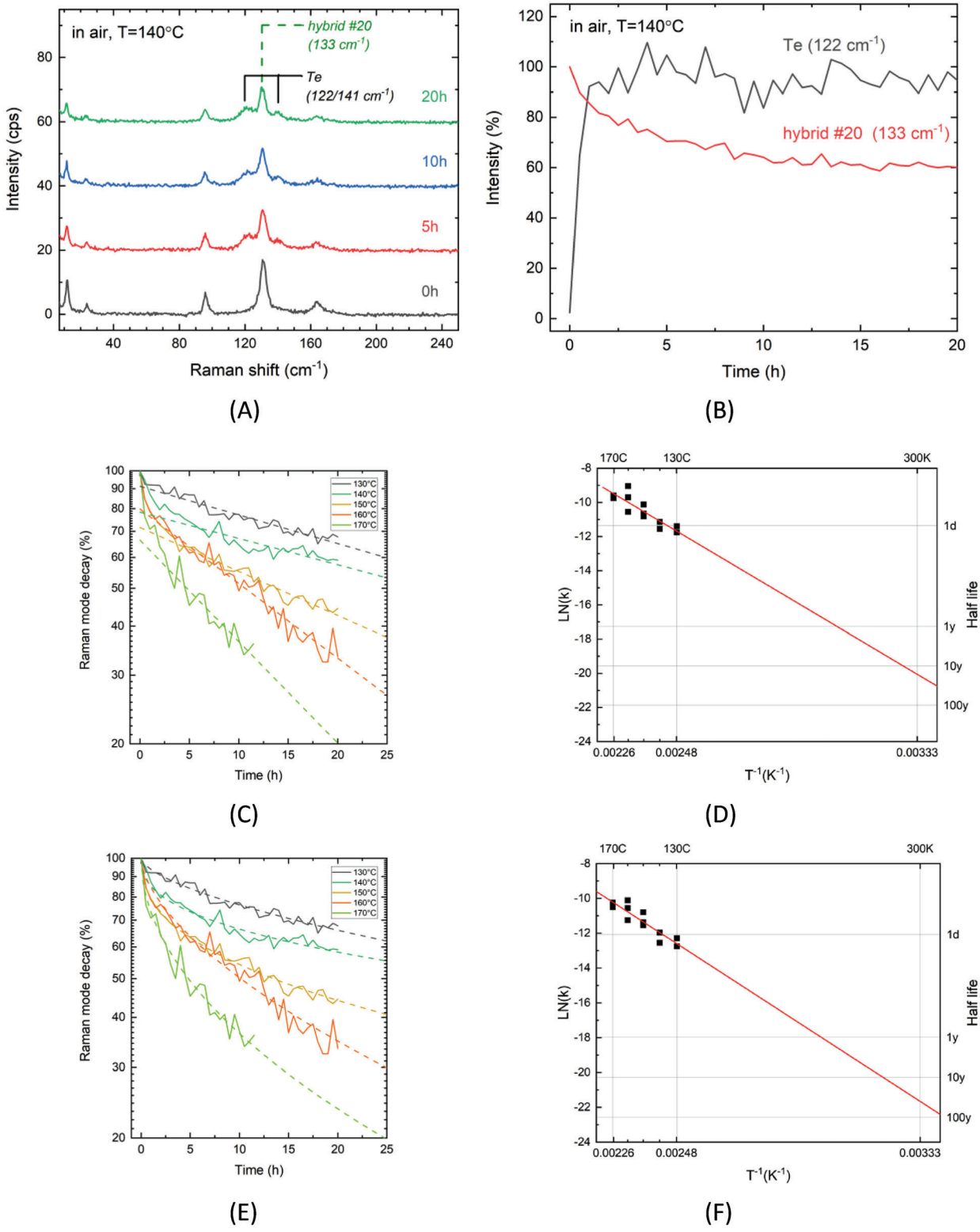

Figure 4. In situ Raman monitoring of thermal degradation of β-ZnTe(en)$_{0.5}$ in air. A) Raman spectra acquired at 1, 5, 10, and 20 h after the hybrid sample is heated to 140 °C. B) The normalized intensity of the hybrid mode #20 (at 133 cm^{-1}) and Te mode (122 cm^{-1}) is plotted against time. C) Normalized Raman peak intensity (hybrid mode #20) versus time, in log scale, at selected temperatures between 130 and 170 °C. Solid lines are peak intensity data acquired in intervals of 5 min, overlapped with fitting curves (dashed lines) using exponential decay. D) The corresponding Arrhenius relationship $k(T)$ versus $1/T$. Right axis labels the half-life corresponding to different values of $\ln(k)$. E) The same data as (C), but fit with stretched exponential. F) The same plot as (D), but for the stretched exponential fit results.

reaction process. In contrast, the tellurium mode growth saturates after 2 h, likely because the excitation wavelength is in the strongly absorptive region of Te and the Raman signal collected is primarily from the top layer. We, therefore, use the Raman decay of the 133 cm^{-1} hybrid mode to monitor reaction progress.

Note that Raman intensity decay of a hybrid mode with oxidation is caused by the growing tellurium because of its high absorbance (6.8×10^5 cm^{-1} at 532 nm),[32] while in intrinsic degradation, it is the collapse of the structure into en molecules and bulk ZnTe leading to the Raman decay. Unlike the case of intrinsic degradation, in which the observed Raman intensity $A_{\text{nitrogen}}(t)$ exhibits exponential decay, the Raman decays in ambient air $A_{\text{air}}(t)$ is nonexponential, as shown in Figure 4C for various temperatures (the complete data set is given in SM3, Figure S2, Supporting Information). We attempt to fit the decay with a stretched-exponential model that is often used to describe more complex biochemical reactions or biological survival curves.[33]

$$\mathrm{A\,(t)} = \exp\left[-(\mathrm{kt})^{\mathrm{b}}\right], \qquad \text{with } 0 < \mathrm{b} < 1 \tag{4}$$

In contrast to the simple exponential decay where a global rate (k) is assumed, the stretched-exponential views the process as a linear combination of different rates, whose weights can be described using a continuous distribution.[34,35] In the expression of the stretched exponential decay [Equation (4)], k describes the effective rate, and b describes the width of the rate distribution. In ambient degradation, accumulation of the tellurium on the sample surface from the early stage of the reaction effectively shields the hybrid from further attack by oxidation agents such as O_2 and H_2O molecules. Under this picture, the rate becomes slower as the reaction progresses. We choose stretched-exponential because it captures the dispersive rate along the different stages of the reaction and thus is expected to give more accurate estimate of lifetime. Using a single exponential, on the other hand, may underestimate the lifetime.

Figure 4C–F depicts the observed Raman decay, fitted with both exponential and stretched exponential. Evidently, the stretched exponential model can fit the full time range nicely, whereas the simple exponential cannot. From each model, the activation barrier (E_A) and the half-life at room temperature $t_{1/2}(T = 300\ \mathrm{K})$ are estimated (SM4, Supporting Information). For the stretched exponential model, the fitting yields $b = 0.49 \pm 0.03$, $E_A = 0.92 \pm 0.13$ eV, and $t_{1/2}(T = 300\ \mathrm{K}) = 40$ (from 8.8 to 183) years; and for the exponential model, $E_A = 0.85 \pm 0.15$ eV and $t_{1/2}(T = 300\ \mathrm{K}) = 17$ (from 3.2 to 90) years. We may take the lower value of the order of 20 years as the lower bound of β-ZnTe(en)$_{0.5}$'s room temperature lifetime, whereas the larger value of the order of 40 years as the lifetime for the optimal conditions, i.e., with passivated edges and defect free surfaces. These values are in accord with the experimental findings: aged samples over 16-year old were often found showing the pristine spectroscopic features with no sign of degradation.[17] The lowered thermal activation barrier (0.92 eV) in ambient conditions, compared with the intrinsic case (1.62 eV), can be understood qualitatively as a catalytic effect provided by O_2 or H_2O that reduces the reaction barrier, because more degradation channels are now available.

3. Conclusion

β-ZnTe(en)$_{0.5}$'s unprecedented ambient long-term stability over 15 years, although still limited by extrinsic mechanisms, is already the longest-lived hybrid semiconductor documented. By monitoring its thermal degradation processes in a protected environment (in N_2) and in air, respectively, we have obtained the activation barrier for the former case to be 1.62 ± 0.08 eV, corresponding to an about 8.2×10^7 years' room temperature lifetime; and the activation barrier for the latter case of 0.92 ± 0.13 eV, corresponding to a 40 years' room temperature lifetime. The measured activation barrier for the intrinsic thermal degradation agrees well with the calculated total energy barrier of the transition state in a proposed one-step decomposition picture, and DFT calculations have revealed the factors contributing to the stability. The projected ambient lifetime is also consistent with the observed shelf life of the material. This work indicates that accelerated thermal aging can indeed offer a fairly reliable methodology to predict the intrinsic and ambient-condition long-term stability of a hybrid material.

While it is easy to understand that the structural distortions of the participating substructures in an organic-inorganic hybrid or any superstructures are expected to increase the formation energy, it has not been explicitly recognized that such distortions are the primary mechanism to form the kinetic barrier that may play a prominent role in the overall structural stability. This study provides new insight for understanding and improving the long-term stability of the hybrid structures.

4. Experimental Section

Materials: β-ZnTe(en)$_{0.5}$ crystals were taken from the batch synthesized in 2019 for a previous study.[17] The synthesis followed a previously reported procedure with slight modifications.[12] $ZnCl_2$ (333 mg, 2 mmol), Te (128 mg, 1 mmol), and ethylenediamine (4 mL) were placed in a Teflon-lined stainless steel high-pressure acid digestion vessel (Parr model 4746). The vessel was placed in a muffle furnace set at 200 °C for 10 d. After slow cooling to room temperature, the resulting product mixture was filtered and washed with distilled water, 95% ethanol, and diethyl ether, then dried in air to produce colorless plate-like crystals.

Optical Characterization: Raman measurements were carried out using a Horiba LabRam HR800 confocal Raman microscope with a 1200 g mm^{-1} grating. A 532 nm laser beam was focused on the sample using a long working distance 50× microscope lens with NA = 0.5. The sample was mounted in a heating system Linkam TS1500, which has a sapphire window for light transmission. When monitoring the reaction process, a ramping rate of 20 °C min^{-1} was used to reach the target temperature, before Raman spectra were taken from the sample in every 5–30 min. Shorter time step was used to resolve the fast rate for higher temperature profiles. To monitor the intrinsic degradation, a mild sustained N_2 gas was flowed into the chamber during the entire temperature-dependent measurements.[36] To study ambient degradation, two gas outlets were open to the ambient air. For both intrinsic degradation and ambient degradation, a baseline time-map at room temperature was acquired and no degradation feature was observed.

Density-Functional Theory Calculations: DFT calculations were carried out using the Vienna ab initio simulation package (VASP).[37] The projector augmented wave potentials were used to describe the interaction between the ion-cores and valence electrons. The PBEsol generalized gradient approximation was used for the exchange–correlation functional. Plane-waves with cutoff energy of 30 Ry were used as basis set. The calculated lattice constants are $a = 5.5838$ Å, $b = 17.2040$ Å, and $c = 4.3236$ Å, which are in good agreement with the measured lattice parameters at

4.2 K:[15] $a = 5.6569$ Å, $b = 17.1983$ Å, and $c = 4.3429$ Å. The formation energy of β-ZnTe(en)$_{0.5}$ was calculated by taking the total energy difference between bulk β-ZnTe(en)$_{0.5}$ and the sum of zinc-blende ZnTe and $C_2N_2H_8$ molecule in the corresponding stoichiometry. ZnTe was calculated in zinc-blende structure and $C_2N_2H_8$ molecule was calculated in a supercell of $17.25 \times 15 \times 15$ Å^3. The accuracy of the formation energy calculation is around 10%.[38] Both isolated (110) two-monolayer ZnTe and en molecule were calculated in two configurations: 1) fully relaxed and 2) the same configuration as in the hybrid.

Supporting Information

Supporting Information is available from the Wiley Online Library or from the author.

Acknowledgements

The work at UNCC was supported by ARO/Physical Properties of Materials (Grant No. W911NF-18-1-0079) and Bissell Distinguished Professorship. The work at SICCAS was supported by Shanghai International Cooperation Project (Grant No. 20520760900).

Conflict of Interest

The authors declare no conflict of interest.

Data Availability Statement

The data that support the findings of this study are available from the corresponding author upon reasonable request.

Keywords

accelerated thermal aging, degradation mechanism, kinetic barriers, micro-Raman spectroscopy, organic–inorganic hybrids

Received: April 7, 2023
Revised: December 12, 2012
Published online:

[1] C. Sanchez, B. Julián, P. Belleville, M. Popall, *J. Mater. Chem.* **2005**, *15*, 3559.
[2] G. Kickelbick, in *Hybrid Materials: Synthesis, Characterization, and Applications* (Ed: K. Guido), Wiley, Darmstadt **2007**, pp. 1–48.
[3] W. Liu, Y. Fang, J. Li, *Adv. Funct. Mater.* **2018**, *28*, 1705593.
[4] S. Yang, S. Chen, E. Mosconi, Y. Fang, X. Xiao, C. Wang, Y. Zhou, Z. Yu, J. Zhao, Y. Gao, F. De Angelis, J. Huang, *Science* **2019**, *365*, 473.
[5] R. Wang, J. Xue, K.-L. Wang, Z. K. Wang, Y. Luo, D. Fenning, G. Xu, S. Nuryyeva, T. Huang, Y. Zhao, J. L. Yang, J. Zhu, M. Wang, S. Tan, I. Yavuz, K. N. Houk, Y. Yang, *Science* **2019**, *366*, 1509.
[6] Y. Wang, T. Wu, J. Barbaud, W. Kong, D. Cui, H. Chen, X. Yang, L. Han, *Science* **2019**, *365*, 687.
[7] Y. Zhao, F. Ma, Z. Qu, S. Yu, T. Shen, H. X. Deng, X. Chu, X. Peng, Y. Yuan, X. Zhang, J. You, *Science* **2022**, *377*, 531.
[8] Y.-Y. Zhang, S. Chen, P. Xu, H. Xiang, X. G. Gong, A. Walsh, S.-H Wei, *Chin. Phys. Lett.* **2018**, *35*, 036104.
[9] E. Smecca, Y. Numata, I. Deretzis, G. Pellegrino, S. Boninelli, T. Miyasaka, A. La Magna, A. Alberti, *Phys. Chem. Chem. Phys.* **2016**, *18*, 13413.
[10] X. Zhao, T. Liu, Q. C. Burlingame, T. Liu, R. Holley, G. Cheng, N. Yao, F. Gao, Y. L. Loo, *Science* **2022**, *377*, 307.
[11] J. Li, R. Zhang, Progress in Inorganic Chemistry, Vol. *57*, First Edition, Ed.: Kenneth D. Karlin, John Wiley & Sons, Inc. Published 2012 by John Wiley & Sons, Inc. **2012**.
[12] X. Huang, J. Li, Y. Zhang, A. Mascarenhas, *J. Am. Chem. Soc.* **2003**, *125*, 7049.
[13] Y. Zhang, *J. Lumin.* **2022**, *248*, 118936.
[14] Y. Zhang, G. M. Dalpian, B. Fluegel, S.-H Wei, A. Mascarenhas, X.-Y. Huang, J. Li, L.-W. Wang, *Phys. Rev. Lett.* **2006**, *96*, 026405.
[15] Y. Zhang, Z. Islam, Y. Ren, P. A. Parilla, S. P. Ahrenkiel, P. L. Lee, A. Mascarenhas, M. J. Mcnevin, I. Naumov, H.-X. Fu, X.-Y. Huang, J. Li, *Phys. Rev. Lett.* **2007**, *99*, 215901.
[16] L. Wang, M. T. Dove, J. Shi, B. Sun, D. Hu, C. Wang, *Dalton Trans.* **2019**, *49*, 719.
[17] T. Ye, M. Kocherga, Y.-Y Sun, A. Nesmelov, F. Zhang, W. Oh, X. Y. Huang, J. Li, D. Beasock, D. S. Jones, T. A. Schmedake, Y. Zhang, *ACS Nano* **2021**, *15*, 10565.
[18] X. Qian, X. Gu, R. Yang, *Nano Energy* **2017**, *41*, 394.
[19] X. Qian, X. Gu, R. Yang, *J. Phys. Chem. C* **2015**, *119*, 28300.
[20] R. L. Forrest, T. D. Golding, S. C. Moss, Y. Zhang, J. F. Geisz, J. M. Olson, A. Mascarenhas, P. Ernst, C. Geng, *Phys. Rev. B* **1998**, *58*, 15355.
[21] J. H. Li, S. C. Moss, Y. Zhang, A. Mascarenhas, L. N. Pfeiffer, K. W. West, W. K. Ge, J. Bai, *Phys. Rev. Lett.* **2003**, *91*, 106103.
[22] F. Zhang, J. F. Castaneda, S. Chen, W. Wu, M. J. Dinezza, M. Lassise, W. Nie, A. Mohite, Y. Liu, S. Liu, D. Friedman, H. Liu, Q. Chen, Y. H. Zhang, J. Huang, Y. Zhang, *Mater. Today* **2020**, *36*, 18.
[23] L. P. Sergei, in *Optoelectronics* (Eds: L. P. Sergei, B. John), IntechOpen, Rijeka **2015**, Ch. 1.
[24] C. Hu, Q. Chen, F. Chen, T. H. Gfroerer, M. W. Wanlass, Y. Zhang, *Light: Sci. Appl.* **2018**, *7*, 23.
[25] M. Yan, C. A. Myers, G. M. John, V. E. Meyers, A. A. Chen, J. I. Feldblyum, *Adv. Mater. Interfaces* **2022**, *9*, 2200347.
[26] J. F. Castaneda, J. H. Im, Y. Liu, S. Liu, N. G. Park, Y. Zhang, *ACS Energy Lett.* **2022**, *7*, 3095.
[27] D. G. Truhlar, B. C. Garrett, S. J. Klippenstein, *J. Phys. Chem.* **1996**, *100*, 12771.
[28] S.-H. Wei, A. Zunger, *Phys. Rev. Lett.* **1988**, *61*, 1505.
[29] A. Poglitsch, D. Weber, *J. Chem. Phys.* **1987**, *87*, 6373.
[30] C. Y. Moon, G. M. Dalpian, Y. Zhang, S.-H Wei, X. Y. Huang, J. Li, *Chem. Mater.* **2006**, *18*, 2805.
[31] Y. Li, J. Yang, R. Zhao, Y. Zhang, X. Wang, X. He, Y. Fu, L. Zhang, *J. Am. Chem. Soc.* **2022**, *144*, 16656.
[32] A. Ciesielski, L. Skowronski, W. Pacuski, T. Szoplik, *Mater. Sci. Semicond. Process.* **2018**, *81*, 64.
[33] B. M. Weon, J. H. Je, *Biogerontology* **2009**, *10*, 65.
[34] A. Plonka, *Lecture Notes in Chemistry*, *vol. 40*, Springer, Berlin, Heidelberg, **1986**, pp. 1–5.
[35] J. Sworakowski, K. Matczyszyn, *Acta Phys. Pol., A* **2007**, *112*, S153.
[36] L. Su, Y. Zhang, *Appl. Phys. Lett.* **2015**, *107*, 071905.
[37] G. Kresse, J. Furthmüller, *Phys. Rev. B: Condens. Matter* **1996**, *54*, 11169.
[38] G. I. Csonka, J. P. Perdew, A. Ruzsinszky, P. H. T. Philipsen, S. Lebègue, J. Paier, O. A. Vydrov, J. G. Ángyán, *Phys. Rev. B* **2009**, *79*, 155107.